

# High-speed photodiodes for InP-based photonic integrated circuits

E. Rouvalis,<sup>1,\*</sup> M. Chtioui,<sup>2</sup> M. Tran,<sup>2</sup> F. Lelarge,<sup>2</sup> F. van Dijk,<sup>2</sup> M. J. Fice,<sup>1</sup> C. C. Renaud,<sup>1</sup> G. Carpintero,<sup>3</sup> and A. J. Seeds<sup>1</sup>

<sup>1</sup>Department of Electronic and Electrical Engineering, University College London, Torrington Place, WC1E 7JE, UK  
<sup>2</sup>III-V Lab, a joint lab of Thales Research and Technology, Alcatel-Lucent Bell Labs France, and CEA Leti, 91767 Palaiseau Cedex, France

<sup>3</sup>Universidad Carlos III de Madrid, Av de la Universidad, 30. Leganes 28911 Madrid, Spain  
[e.rouvalis@ee.ucl.ac.uk](mailto:e.rouvalis@ee.ucl.ac.uk)

**Abstract:** We demonstrate the feasibility of monolithic integration of evanescently coupled Uni-Traveling Carrier Photodiodes (UTC-PDs) having a bandwidth exceeding 100 GHz with Multimode Interference (MMI) couplers. This platform is suitable for active-passive, butt-joint monolithic integration with various Multiple Quantum Well (MQW) devices for narrow linewidth millimeter-wave photomixing sources. The fabricated devices achieved a high 3-dB bandwidth of up to 110 GHz and a generated output power of more than 0 dBm (1 mW) at 120 GHz with a flat frequency response over the microwave F-band (90–140 GHz).

©2012 Optical Society of America

**OCIS codes:** (250.5300) Photonic integrated circuits; (040.5160) Photodetectors; (060.5625) Radio frequency photonics.

---

## References and links

1. H.-J. Song and T. Nagatsuma, "Present and future of terahertz communications," *IEEE Trans. Terahertz Sci. Tech.* **1**(1), 256–263 (2011).
2. A. Stöhr, P. Cannard, B. Charbonnier, F. van Dijk, S. Fedderwitz, D. Moodie, L. Pavlovic, L. Ponnampalam, C. C. Renaud, D. Rogers, V. Rymanov, A. Seeds, A. Steffan, A. Umbach, and M. Weiß, "Millimeter-wave photonic components for broadband wireless systems," *IEEE Trans. Microw. Theory Tech.* **58**(11), 3071–3082 (2010).
3. M. J. Fice, E. Rouvalis, F. van Dijk, A. Accard, F. Lelarge, C. C. Renaud, G. Carpintero, and A. J. Seeds, "146-GHz millimeter-wave radio-over-fiber photonic wireless transmission system," *Opt. Express* **20**(2), 1769–1774 (2012).
4. M. J. Fice, E. Rouvalis, L. Ponnampalam, C. C. Renaud, and A. J. Seeds, "Telecommunications technology-based terahertz sources," *Electron. Lett.* **46**(26), S28–S31 (2010).
5. E. Rouvalis, C. C. Renaud, D. G. Moodie, M. J. Robertson, and A. J. Seeds, "Traveling-wave uni-traveling carrier photodiodes for continuous wave THz generation," *Opt. Express* **18**(11), 11105–11110 (2010).
6. J.-W. Shi, F.-M. Kuo, C.-J. Wu, C. L. Chang, C.-Y. Liu, C. Y. Chen, and J.-I. Chyi, "Extremely high saturation current-bandwidth product performance of a near-ballistic uni-traveling-carrier photodiode with a flip-chip bonding structure," *IEEE J. Quantum Electron.* **46**(1), 80–86 (2010).
7. M. Chtioui, F. Lelarge, A. Enard, F. Pommereau, D. Carpentier, A. Marceaux, F. Van Dijk, and M. Achouche, "High responsivity and high power UTC and MUTC GaInAs-InP photodiodes," *IEEE Photon. Technol. Lett.* **24**(4), 318–320 (2012).
8. J. Klamkin, A. Ramaswamy, H.-F. Chou, M. N. Sysak, J. W. Raring, N. Parthasarathy, S. P. DenBaars, J. E. Bowers, and L. A. Coldren, "Monolithically integrated balanced uni-traveling-carrier photodiode with tunable MMI coupler for microwave photonic circuits," in *Proc. Conf. Optoelectron. Microelectron. Materials Devices (COMMAD)* 2006, 184–187.
9. S. S. Agashe, S. Datta, F. Xia, and S. R. Forrest, "A monolithically integrated long-wavelength balanced photodiode using asymmetric twin-waveguide technology," *IEEE Photon. Technol. Lett.* **16**(1), 236–238 (2004).
10. S. Murthy, M. C. Wu, D. Sivco, and A. Y. Cho, "Parallel feed travelling wave distributed pin photodetectors with integrated MMI couplers," *Electron. Lett.* **38**(2), 78–80 (2002).
11. A. Beling and J. C. Campbell, "InP-based high-speed photodetectors," *J. Lightwave Technol.* **27**(3), 343–355 (2009).
12. J. W. Raring, E. J. Skogen, C. S. Wang, J. S. Barton, G. B. Morrison, S. Demiguel, S. P. Denbaars, and L. A. Coldren, "Design and demonstration of novel QW intermixing scheme for the integration of UTC-type photodiodes with QW-based components," *IEEE J. Quantum Electron.* **42**(2), 171–181 (2006).
13. E. Rouvalis, C. C. Renaud, D. G. Moodie, M. J. Robertson, and A. J. Seeds, "Continuous wave terahertz generation from ultra-fast InP-based photodiodes," *IEEE Trans. Microw. Theory Tech.* **60**(3), 509–517 (2012).

- 
14. C. C. Renaud, D. Moodie, M. Robertson, and A. J. Seeds, "High output power at 110 GHz with a waveguide uni-travelling carrier photodiode," in *Proc. 20th Ann. Meeting IEEE Lasers and Electro-Optics Soc. (LEOS) 2007*, 782–783.
- 

## 1. Introduction

Broadband wireless communications have recently seen significant evolution, especially where data rates over 1 Gbps are required. Several competing technologies have been proposed [1]. In the 60 GHz band, wireless transmission based on optoelectronic technology has been demonstrated successfully [2]. However, the demand for even higher data rates will eventually push the carrier frequencies towards the 120 GHz band [3]. Photomixing in high speed photodiodes in combination with injection and phase locking techniques is one of the most promising techniques for the generation of high power, narrow linewidth millimeter-wave signals [4]. A key component in these systems is the high speed photodiode. Uni-Traveling Carrier Photodiodes (UTC-PDs) have been the dominant type of photodiodes for these applications due to their wide bandwidth and high millimeter-wave output power levels [5–7].

A major drawback of photomixing systems can be the overall power consumption that can be partially attributed to fibre-to-chip coupling losses. High speed photodiodes are typically grown with thin absorption layers and coupling light from an optical fiber can become challenging. The majority of high speed, high responsivity photodiodes are fabricated in a waveguide configuration where high responsivity and traveling wave operation can be achieved. Thus, another important loss factor is the polarization dependence of the input waveguide, requiring careful polarization matching of the input heterodyne signal. Monolithically integrated photomixing sources can improve the overall power efficiency of the system and may result in extremely compact and low-cost systems. For this purpose, integration of Distributed Feedback (DFB) lasers with tunable phase sections, Electro-Absorption Modulators (EAMs), Semiconductor Optical Amplifiers (SOAs) and Multimode Interference (MMI) couplers can offer a solution for efficient generation of an optical heterodyne signal that can be used as an input to a high bandwidth photodiode. Previous work demonstrated monolithic integration of p-i-n photodetectors and MMI couplers either for balanced photodetectors [8], [9] or for parallel-fed traveling wave photodiodes [10], [11]. Monolithic integration of Multiple Quantum Well (MQW)-based devices has been demonstrated using several different techniques. Despite the high quality lasers, amplifiers and modulators that can be produced, UTC-PDs fabricated using this approach have shown rather low 3-dB bandwidth [12]. To further improve the functionality of PICs, the technology of integrating MQW-based devices with high speed photodiodes must be developed.

Here we demonstrate high speed ( $f_{3\text{dB}} > 100 \text{ GHz}$ ) UTC-PDs based on epitaxial regrowth in a Multiple Quantum Well platform with a cap layer of 1  $\mu\text{m}$ . The devices achieved a generated output power of 1 mW at 120 GHz. An average loss of 2.6 dB/mm in the passive sections was measured and different MMI coupler designs were assessed. We expect this technology to lead to photomixing PICs for 10 Gb/s wireless transmission at 120 GHz.

## 2. UTC-PD design challenges

In most common, stand-alone UTC-PDs the p-contact layer, which is also used as a diffusion blocking layer, has a typical thickness of a few hundred nm. The technology that is used to integrate active and passive photonic devices requires the regrowth of a thick, highly doped InP layer on top of the UTC-PD layers that also serves as a diffusion blocking layer. This InP layer is followed by p-contact layers. To achieve low propagation loss in the passive sections and avoid excessive losses in p-contact layers, the InP cap layer has to be relatively thick. However, this will increase the series resistance of the photodiode and will result in a low RC-limited bandwidth.

The propagation loss in the passive sections for a waveguide with a length of 1 mm as a function of the cap layer thickness was modeled with RSoft and is plotted in Fig. 1(a), together with the modeled series resistance  $R_s$  for a  $2 \times 15 \mu\text{m}^2$  and  $3 \times 15 \mu\text{m}^2$  photodiodes

and the layer stack for these simulations is given in the inset. When the thickness of the cap layer is of the order of 0.5  $\mu\text{m}$  the propagation loss becomes extremely high. On the other hand, for very thick cap layers ( $>1.3 \mu\text{m}$ ) the propagation loss does not vary significantly. However, in this case, the series resistance increases significantly ( $>30 \Omega$  for the  $2 \times 15 \mu\text{m}^2$  device) which will limit the photodiode RC-bandwidth. Therefore, a thickness of 1  $\mu\text{m}$  was chosen as a compromise between propagation losses and high series resistance.

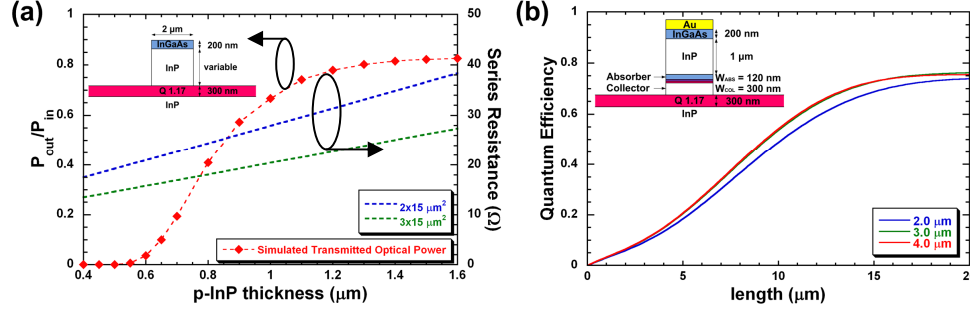


Fig. 1. (a) Output optical power divided by input optical power after propagation over 1 mm ( $\lambda = 1.55 \mu\text{m}$ ), together with simulated series resistance as a function of cap layer thickness. (b) Quantum Efficiency of waveguide UTC-PDs ( $\lambda = 1.55 \mu\text{m}$ ) versus length of the device for 3 different widths (2, 3 and 4  $\mu\text{m}$ ).

To find the optimum active area dimensions, the device was modeled using a semi-analytical model that is described in [5] and [13]. The optical absorption in the device was modeled using FIMMWAVE. The optical signal is evanescently coupled from the passive waveguide layer in to the absorber of the UTC-PD. The predicted quantum efficiency as a function of the device length for various device widths is shown in Fig. 1(b) while the epitaxy of the UTC-PD with a 1  $\mu\text{m}$  cap layer is given in the inset. It can be seen that the device width does not affect the quantum efficiency significantly. For lengths above 15  $\mu\text{m}$  the quantum efficiency increases only marginally while the capacitance increases by a factor that is proportional to the length of the device. This result was used as an input to a semi-analytical model that predicts the frequency response of the UTC-PD. The model is a combination of a Transmission Line Model with carrier transport drift-diffusion model that predicts the extrinsic and the intrinsic response of the device respectively. A constant arbitrary level of optical power was assumed as an input to the device. The optimization function was set as the maximum output power at 120 GHz with the length and the width of the device being variable. The normalized power delivered to a 50  $\Omega$  load is shown in Fig. 2.

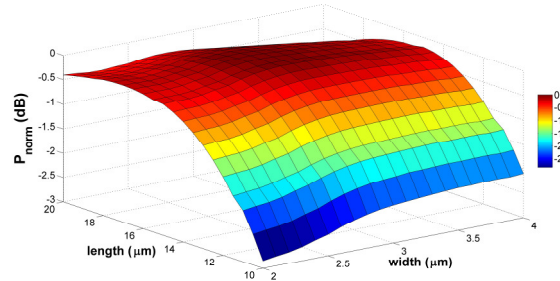


Fig. 2. Normalized generated power at 120 GHz as a function of device length and width.

The combination of dimensions that resulted in the maximum generated power was 3.2  $\mu\text{m} \times 15 \mu\text{m}$ . When the device is made shorter than 15  $\mu\text{m}$ , the generated power is mainly limited by the lower quantum efficiency and saturation and thermal effects. Devices longer than 15  $\mu\text{m}$  suffer from a higher capacitance that limits the frequency response. For narrow

devices saturation will occur at a lower photocurrent level but when the width exceeds  $3.2\text{ }\mu\text{m}$  the device becomes RC limited. For practical purposes in the mask design, the optimum device dimensions were considered as  $3\text{ }\mu\text{m} \times 15\text{ }\mu\text{m}$ . These active area dimensions resulted in a simulated series resistance of about  $20\text{ }\Omega$  that is an acceptable value for a UTC-PD with a thick cap layer.

### 3. Growth and fabrication

The developed UTC-PDs, shown in Fig. 3, are fabricated on a semi-insulating InP substrate using gas source molecular beam epitaxy. For the fabrication of these devices we implemented monolithic integration of passive waveguides and optical couplers, and photodiode active sections. This was done with two epitaxial growth steps. The first epitaxial step is for the growth of passive waveguide and PD absorber and collector layers. Then, during the second epitaxial step, an overall regrowth of top p-InP cladding and p-contact layers is performed. The process flow of our integrated UTC-PDs fabrication is then mainly based on dry and wet etching for the realization of shallow ridge waveguides, PD mesa, and PD isolation. Finally, a BCB planarization step is performed, followed by a metallization step for electrode interconnection. This process flow uses fabrication steps that are compatible with the integration of MQW active sections and the realization of shallow ridge laser and SOA waveguides.

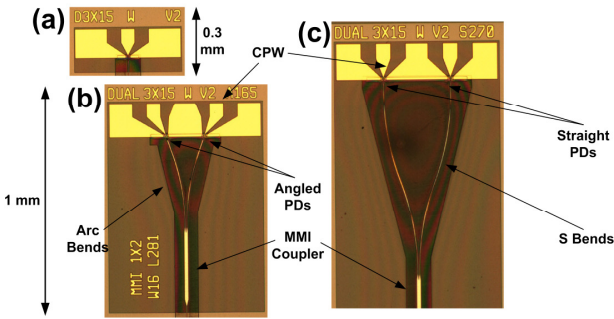


Fig. 3. Images of chips with (a) Single UTC-PDs, (b) Dual angled UTC-PDs with Arc-Type bends and (c) Dual straight UTC-PDs with S-type bends.

### 4. Single photodiodes

Single UTC-PDs were fabricated with a p-doped,  $1\text{-}\mu\text{m}$  cap layer. The optimum active area dimensions were taken as  $3 \times 15\text{ }\mu\text{m}^2$ . To make a comparison with the modelling results, devices with all possible combinations of widths ( $2, 3$  and  $4\text{ }\mu\text{m}$ ) and lengths ( $10, 15$  and  $20\text{ }\mu\text{m}$ ) were also fabricated. The performance of the UTC-PDs was measured on chips with single devices (Fig. 3(a)). The series resistance for  $3 \times 15\text{ }\mu\text{m}^2$  devices was found to be about  $20\text{ }\Omega$  and the capacitance was found to be  $18\text{ fF}$ . The resulting RC-limited bandwidth is about  $125\text{ GHz}$  while the modelled transit-time limited bandwidth was  $165\text{ GHz}$ , resulting in a total bandwidth of about  $90\text{ GHz}$ . A lensed fiber with a  $3\text{ }\mu\text{m}$  spot size was used for all measurements and a responsivity of  $0.35\text{ A/W}$  at  $1.55\text{ }\mu\text{m}$  was found for UTC-PDs with a length of  $15\text{ }\mu\text{m}$ . It is noteworthy that the tested devices do not have anti-reflection coating. The frequency response from single UTC-PDs grown and fabricated with the technique described in the previous section was assessed using two External Cavity Lasers (ECLs), coplanar waveguide probes and a calibrated power meter that operates up to  $110\text{ GHz}$ . The frequency response for devices with various dimensions is given in Fig. 4(a). A  $3\text{-dB}$  bandwidth between  $80$  and  $110\text{ GHz}$  was measured depending on the device active area dimensions. All measurements were taken at a photocurrent of  $5\text{ mA}$  to ensure that the frequency response was not affected by power saturation effects.

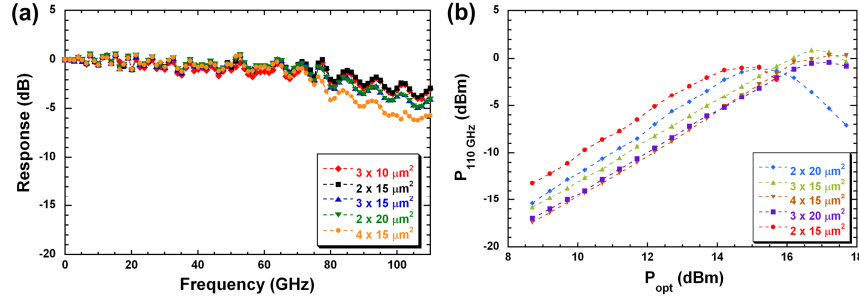


Fig. 4. (a) Normalized frequency response up to 110 GHz from UTC-PDs with various active area dimensions. All measurements were taken at a DC photocurrent level of 5 mA. (b) Power saturation at 110 GHz for various UTC-PDs with different active area dimensions. The reverse bias voltage was 3 V.

To investigate saturation effects, the generated millimeter-wave power at the maximum frequency of operation of the power meter (110 GHz) as a function of the optical input power was measured and the results are shown in Fig. 4(b). The  $3 \times 15 \mu\text{m}^2$  UTC-PDs demonstrated the maximum level of output power with 1 dBm at 110 GHz. The measurements in Fig. 4(b) are corrected for the insertion loss of the coplanar probe (0.8 dB at 110 GHz). Despite the small difference in the frequency, a remarkable agreement between theory and experiment was observed, especially as far as the maximum generated power is concerned. Devices with a smaller active area than the optimum saturated at a lower photocurrent level, while larger devices were found to be RC-limited. UTC-PDs are known to have higher saturation power and we believe that for the devices reported here the introduction of a higher series resistance is the main cause for lower measured power than previously reported [14].

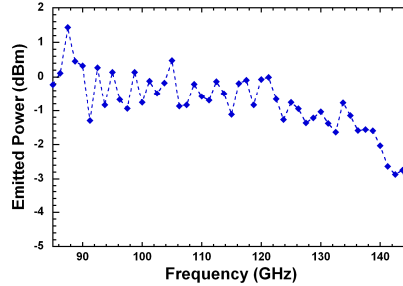


Fig. 5. Emitted power from a  $3 \times 15 \mu\text{m}^2$  UTC-PD in the F-Band (90-140 GHz). The DC photocurrent level was 12 mA.

For power measurements in the F-band (90-140 GHz) a probe with a WR-8 rectangular waveguide output was used. A 20 dBi-gain horn antenna was connected at the output of the waveguide and the power of the generated signal was measured using a free space Terahertz power meter. More details about this experimental arrangement can be found in [13]. The emitted power in the F-band from a  $3 \times 15 \mu\text{m}^2$  UTC-PD is plotted in Fig. 5. A 0 dBm signal was measured at 120 GHz with power fluctuations remaining within 3 dB over the entire F-band. It is noteworthy that the insertion loss of the probe was not taken into account in this measurement.

## 5. Dual photodiodes

Chips with dual photodiodes and  $1 \times 2$  MMI couplers were also assessed (Fig. 3(b), 3(c)). The purpose of these PICs was to assess simultaneously the use of one UTC-PD as a millimeter-wave source and another one as a LO driving source for a mixer incorporated in a phase locked loop circuitry. Single photodiodes with the same chip length were included in the mask in order to evaluate the propagation loss independently from the insertion loss introduced from the MMI coupler and the Arc-type (Fig. 3(b)) and S-type (Fig. 3(c)) waveguide bends.

The responsivity at 1.55  $\mu\text{m}$  of devices with chip lengths of 770  $\mu\text{m}$ , 970  $\mu\text{m}$ , and 1170  $\mu\text{m}$  was compared to the one found from single devices with a short input waveguide (70  $\mu\text{m}$ ). The photocurrent at the same optical power level (36 mW) for devices with the same active area dimensions is plotted in Fig. 6(a). By comparing the results at the maximum applied reverse bias, an average propagation loss of 2.6 dB/mm was found from these measurements. Three types of dual  $3 \times 15 \mu\text{m}^2$  photodiode chips were assessed. The first one included Arc-type bends and angled photodiodes to minimize the chip area and the other two included S-type bends and angled and straight photodiodes respectively. The total insertion loss (MMI + bends) was found to be 3.2 dB, 3.6 dB and 4.3 dB respectively -in excess of the 3 dB of the coupler- by comparing the measured responsivity with that for single devices with the same chip length. This relatively high insertion loss can be attributed to the relatively thin cap layer (1  $\mu\text{m}$ ) that was used to achieve a compromise between low optical loss in the passive sections and acceptable series resistance in the PDs.

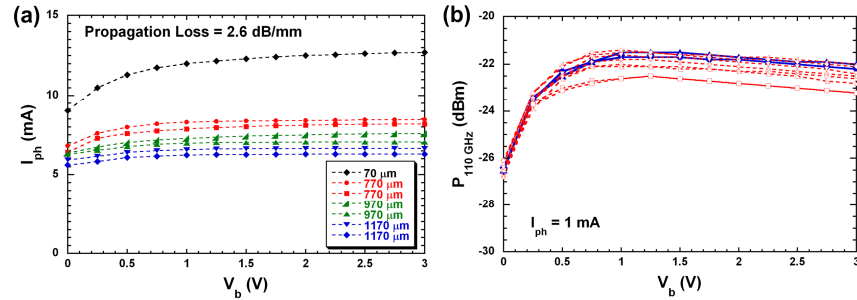


Fig. 6. (a) Photocurrent as a function of applied reverse bias for devices with short (70  $\mu\text{m}$ ) and long waveguides (770  $\mu\text{m}$ , 970  $\mu\text{m}$ , and 1170  $\mu\text{m}$ ) at an input optical power level of 36 mW. The active area of all UTC-PDs was  $3 \times 15 \mu\text{m}^2$ . (b) power at 110 GHz for straight (blue, continuous line) and angled (red, dashed line) UTC-PDs.

In order to investigate the effect of the angled photodiodes and Coplanar Waveguides on the frequency response of the UTC-PDs, the generated output power at 110 GHz was measured from straight and angled photodiodes at the same photocurrent level (1 mA). The results are plotted in Fig. 6(b). An additional average loss of only 0.5 dB at 110 GHz was measured from the angled photodiodes.

## 6. Conclusions

We have demonstrated a technology for active-passive monolithic integration of high speed photodiodes with MQW-based photonic devices. UTC-type photodiodes were designed for high power generation in the microwave F-band (90-140 GHz) despite the high series resistance from the re-grown of thick InP cap layer that should be present to reduce propagation losses in passive MMI and waveguide sections. The fabricated devices achieved 3-dB bandwidth of up to 110 GHz and a generated output power of 0 dBm at 120 GHz. PICs with dual photodiodes and MMI couplers demonstrated losses of 2.6 dB/mm in passive sections. The total insertion loss from MMI coupler and waveguide bending were limited to 4.3 dB. We expect this technology not only to lead to photomixing PICs for wireless communications in the 120 GHz range but also to provide a generic technology platform for PICs that require photodiodes with a 3-dB bandwidth exceeding 100 GHz.

## Acknowledgments

This work was supported by the European Commission within the framework of the European project iPHOS (grant agreement no: 257539). The authors would like to thank Genevieve Glastre for useful discussions. E. Rouvalis acknowledges support by the EPSRC under the EPSRC Doctoral Prize Fellowship scheme. G. Carpintero, on Sabbatical leave at University College London, acknowledges support by Fundación Caja Madrid through a mobility grant.